Chaos, Solitons and Fractals 179 (2024) 114461

Contents lists available at ScienceDirect

Chaos, Solitons and Fractals

journal homepage: www.elsevier.com/locate/chaos

Topological star junctions: Linear modes and solitons

Yaroslav V. Kartashov [a], Vladimir V. Konotop [b,*]

[a] Institute of Spectroscopy, Russian Academy of Sciences, Troitsk, Moscow, 108840, Russia
[b] Departamento de Física and Centro de Física Teórica e Computacional, Faculdade de Ciências, Universidade de Lisboa, Campo Grande, Ed. C8, Lisboa 1749-016, Portugal

ARTICLE INFO

Keywords:
Star-junctions
Su–Schrieffer–Heeger chain
Nonlinearity
Edge states
Topological solitons

ABSTRACT

We address continuous two-dimensional (2D) star-junctions formed by different numbers of Su–Schrieffer-Heeger (SSH) chains that have one common waveguide in the center of the junction. We show that by changing waveguide shifts in the dimers forming individual SSH chains, one can create a rich variety of modes in the center of the junction. Independently of the relation between non-equal bonds of the SSH chains, the in-gap modes localized in the center of the junction can be considered as topological, either representing extensions of the conventional topological edge stages or being modes induced by a defect at one of the SSH chain edges. Degeneracy of the eigenvalues and structure of the localized modes of fully 2D junctions depend on their symmetry and number of chains, and are different from their 1D counterparts obtained in the tight-binding approximation. In the presence of the focusing nonlinearity of the medium such states give rise to families of solitons with distinct stability properties depending on the number of chains in junction, waveguide shifts, and mode symmetry.

1. Introduction

Waveguide arrays, *alias* star-junctions, representing several rays connected with each other through a central site were considered in diverse areas of physics, including optics where they were studied theoretically [1–3] and experimentally [4,5], physics of Bose–Einstein condensates [6], and in the frameworks of general lattice models [7,8]. Furthermore, linear and nonlinear junctions represent building blocks for quantum graphs, on which rich dynamics can be considered [9–13]. Gain guiding junctions [14] and non-Hermitian star-junctions [15] were considered too.

Among the models of junctions explored so far one can distinguish continuous and discrete ones. In the former case the centers (alias edges, vertices, or knots) of the junctions are linked by the continuous bonds described, say, by one-dimensional (1D) linear or nonlinear Schrödinger equations. In the second case the bonds are governed by the discrete equations and corresponding systems describe coupled discrete 1D arrays. Most of the studies of star-junctions dealt with the simplest case, where all bonds in each ray coupled to the central site (or several sites forming the central cluster) are equal. At the same time, it is well known that individual rays may display rather unusual properties, when topological effects are introduced by unequal alternating coupling strengths between the neighboring sites. The Su–Schrieffer–Heeger (SSH) model [16] is the most explored example of such a topological system. Considering permanently growing interest to such structures in topological photonics [17–19], it is natural to address the properties of star-junctions assembled from topologically nontrivial chains representing junction rays. This question has been briefly touched in the literature. In particular two coupled (non-Hermitian) SSH chains considered theoretically [20] and experimentally [21,22] can be viewed as the simplest junction of two rays. In [23] the junctions assembled of two crossing SSH chains were studied. Meantime, complex 2D star-junctions with multiple rays with various discrete rotational symmetries have never been considered in either linear or nonlinear settings.

It is known that even in lattices having simpler configuration than star-junctions, inclusion of nonlinearity may bring unusual and intriguing new features into behavior of topological systems based on waveguide arrays. In particular, self-action in such systems may result in the formation of self-sustained hybrid states – topological solitons – that bifurcate from linear topological modes [24–34] and that were experimentally observed in various topological systems including Floquet [35–37] and higher-order insulators [38–40]. Nonlinear effects in single topological SSH chains were studied in [41–49].

In this work we investigate *nonlinear* star-junctions with different number of rays which, being considered separately, represent SSH chains. Several essential differences of the system considered here clearly distinguishing it from previously considered discrete coupled

* Corresponding author.
E-mail addresses: kartashov@isan.troitsk.ru (Y.V. Kartashov), vvkonotop@ciencias.ulisboa.pt (V.V. Konotop).

https://doi.org/10.1016/j.chaos.2024.114461
Received 21 November 2023; Accepted 3 January 2024

chains should be emphasized. Discrete star-junctions obtained in the tight-binding approximation from the mathematical point of view are multi-component one-dimensional systems, where each configuration is described by a multi-component vector, components of which are the field amplitudes in the arrays. Here we consider truly two-dimensional (2D) model, where the one-component field solves the 2D linear or nonlinear Schrödinger equation. While some properties of this system can be predicted on the basis of the tight-binding approximation [10,11], the difference between continuous system studied here and discrete simplifications remain significant. Namely, in the fully 2D model the eventual symmetry of the array becomes an important factor affecting the degeneracy of modes, the number of guided modes differs from the 1D discrete counterpart and becomes dependent on the waveguide parameters, the stability of the truly 2D nonlinear modes is not predicted by the tight-binding approximations, and even the tight-binding approximation itself poorly describes the physical situation when the number of rays in star-junction increases (because strong overlap of rays in the center of the junction comes into play in this case).

The paper is organized as follows. In Section 2 we formulate the model and discuss relevant physical parameters. Basic predictions on the mode structure and topology are presented using the discrete analog in Section 3. The full scale numerical studies of the 2D NLS equation modeling star-junctions with three, four, and five rays are reported in Section 4. Families of solitons and their stability are presented in Section 5. The outcomes of this analysis are summarized in Conclusion.

2. The model

We consider propagation of a light beam along the z axis in a nonlinear focusing medium with transverse shallow modulation of the refractive index defining star-shaped topological star-junction. The dynamics is described by the nonlinear Schrödinger (NLS) equation for the dimensionless amplitude of the light field ψ

$$i\frac{\partial\psi}{\partial z} = -\frac{1}{2}\Delta\psi - \mathcal{R}(\boldsymbol{r})\psi - |\psi|^2\psi \tag{1}$$

where $\Delta = \partial^2/\partial x^2 + \partial^2/\partial y^2$ and $\boldsymbol{r} = (x, y)$. We are interested in star-junctions assembled of K rays located in space with equal angular spacing $2\pi/K$ between neighbors. Each star-junction obeys $K-$fold discrete rotational symmetry while each ray in it contains N pairs of waveguides (dimers) including central waveguide. The function representing optical potential

$$\mathcal{R}(\boldsymbol{r}) = p\sum_{k=1}^{K} Q_k(\boldsymbol{r}) - p(K-1)e^{-\boldsymbol{r}^2/d^2} \tag{2}$$

is considered for $p > 0$, where each ray represents an SSH chain modeled by

$$Q_k = e^{-\eta_k^2/d^2}\sum_{j=0}^{N-1}\left[e^{-(\xi_k-2aj+a+2s)^2/d^2} + e^{-(\xi_k-2aj)^2/d^2}\right]. \tag{3}$$

Here $\xi_k = x\cos\alpha_k + y\sin\alpha_k$, $\eta_k = y\cos\alpha_k - x\sin\alpha_k$, $\alpha_k = 2\pi(k-1)/K$, d is the width of the individual waveguide $pe^{-\boldsymbol{r}^2/d^2}$, $2a$ is the spacing between neighboring dimers (cells) in the presence of the shift $s \neq 0$, such that $s = 0$ corresponds to the non-dimerized limit, where the distance between all waveguides is identical and is equal to a, $p = (2\pi r_0/\lambda)^2\delta nn$ is the dimensionless depth of an individual waveguide, n is background refractive index and δn is the refractive index contrast, λ is the wavelength. Thus, all SSH chains share a common central waveguide $pe^{-\boldsymbol{r}^2/d^2}$, the total number of waveguides in a junction is $N_{\rm tot} = 2NK - K + 1$, and the discrete rotational symmetry group of the system is the dihedral group D_K. The examples of star-junctions with $K = 3, 4$, and 5 rays with $s = 0$ are presented in left outermost panels (a) of Figs. 2–4.

The introduced optical potential, considered as a defect embedded in a homogeneous linear medium, is known to sustain at least one guided mode for any magnitude of $p > 0$ [50,51]. On the other hand, each of the individual waveguides, when isolated, supports one guided mode for parameters considered here. Thus, by increasing the depth p from zero to a certain finite value, one can achieve the regime, where the total number of the propagation constants of the guided modes in the entire star-junction is exactly equal to $N_{\rm tot}$. Below in this paper we concentrate namely on this regime that allows reliable comparison of the results obtained in the frames of our continuous model with results of the tight-binding approach, on the one hand, and that corresponds to typical experimental situation (in terms of parameters of the array), on the other hand.

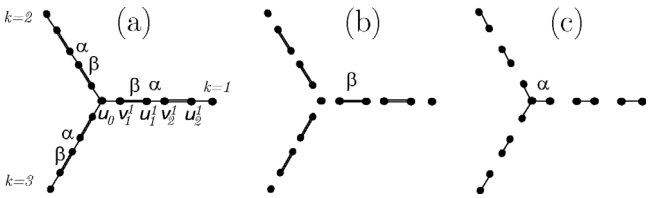

Fig. 1. (a) Example of a discrete star-junction for $K = 3$. (b) and (c) Fully dimerized limits corresponding to $\alpha = 0$ and $\beta = 0$.

Thus, in our model the transverse and longitudinal coordinates (i.e., $\boldsymbol{r}$ and z) are normalized to the characteristic scale $r_0 = 10$ μm and diffraction length $2\pi nr_0^2/\lambda$, respectively, where $\lambda = 800$ nm is the working wavelength. Further, in numerical simulations we set waveguide depth $p = 5$ (this corresponds to refractive index contrast of $\delta n \approx 5.6\times10^{-4}$), spacing $a = 3$ (corresponding to 30 μm), and width $d = 0.5$ (corresponding to 5 μm). Such arrays can be written in transparent dielectrics, such as fused silica, using well-established fs-laser writing technology [52].

3. Discrete star-junctions

Since the chosen regime of operation of star-junctions is somewhat close to the tight-binding limit, we start with a discrete model corresponding to our system. We emphasize, however, that unlike in conventional 1D (or 2D) arrays, now the applicability of the tight-binding limit can be violated in the center of the junction (even if it works well for individual rays far from the center), especially for $s > 0$, when the density of the waveguides and therefore the evanescent mode coupling increases in the center of the junction. Therefore, in this section we intend to provide qualitative analytical description of the spectrum of star-junction with SSH rays, while rigorous numerical modeling of continuous Eq. (1) will be presented in the next section.

Thus, we consider the simplest discrete star-junction, whose schematic illustration is provided in Fig. 1. In this section the rays are considered semi-infinite and we are interested only in modes localized in the center of the junction. For the coupling between nearest neighbors we use parameters α and β, as denoted in Fig. 1. The cases $\alpha < \beta$, $\alpha = \beta$, and $\alpha > \beta$ correspond, respectively, to shifts $s > 0$, $s = 0$, and $s < 0$ introduced above. Without loss of generality we fix $\alpha \geq 0$ and $\beta \geq 0$. We use u_n^k and v_n^k for the fields on the $n-$th cell of the $k-$th ray: $k = 1, 2, \ldots, K$. To the central site we attribute $n = 0$ (without the upper index k), while the cells in the arrays are numbered by $n = 1, 2, \ldots$, as this is explained in Fig. 1(a). For $\alpha = \beta$ (i.e. for equal spacing between all waveguides) such array was considered in [7].

The introduced junction is described by the system

$$i\frac{du_0}{dz} = \alpha(v_1^1 + v_1^2 + \cdots + v_1^K) \tag{4a}$$

$$i\frac{dv_1^k}{dz} = \alpha u_0 + \beta u_1^k, \tag{4b}$$

$$i\frac{dv_n^k}{dz} = \alpha u_{n-1}^k + \beta u_n^k, \qquad n \geq 2 \tag{4c}$$

$$i\frac{du_n^k}{dz} = \beta v_n^k + \alpha v_{n+1}^k, \qquad n \geq 1 \tag{4d}$$

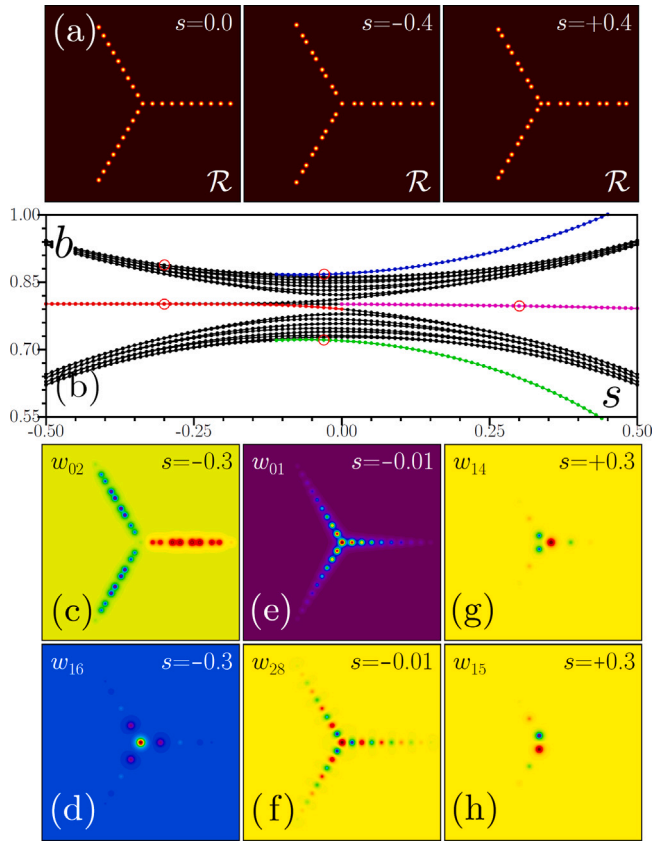

Fig. 2. (a) Examples of star-shaped SSH waveguide arrays with $K = 3$ rays and $N = 5$ dimers in each ray for different values of shift s. (b) Linear spectrum of the array versus waveguide shift s. (c)–(h) Profiles of different linear modes of the array corresponding to red circles in (b). The value of the shift and mode index are indicated on each panel. Profiles of modes are shown within $x, y \in [-30, +30]$ window. For numbering of the modes see the text.

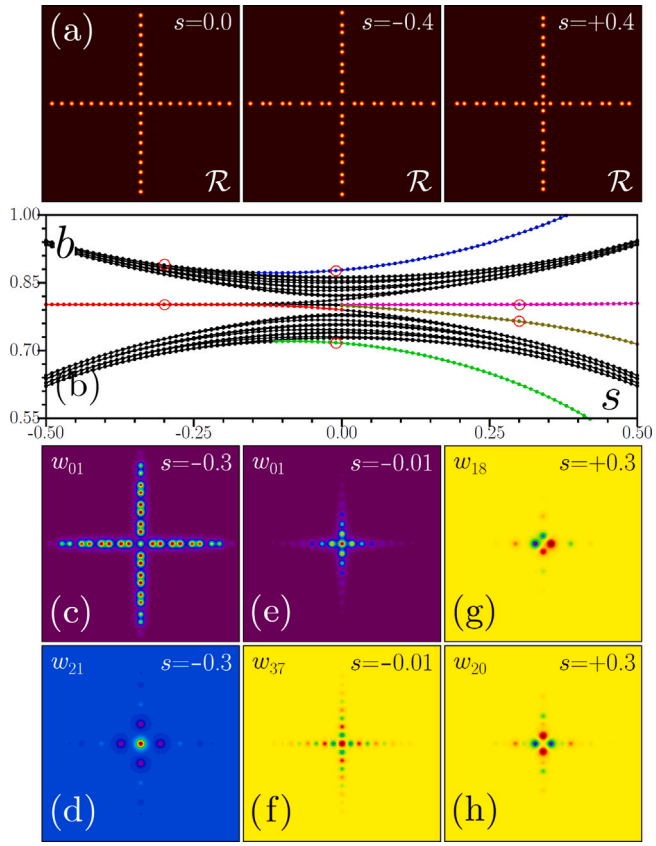

Fig. 3. Examples of arrays with $K = 4$ rays and $N = 5$ dimers (a), transformation of linear spectrum with shift s (b), and examples of eigenmodes (c)–(h).

The simplest way to understand expected features of the introduced star-junctions is to consider their fully dimerized limits [53], shown in Figs. 1(b) and 1(c). One observes that modes localized in the center can exist in both cases: $\alpha = 0$ and $\beta = 0$. At $\alpha = 0$ [panel (b)], representing the limiting case of fully dimerized rays in topological phase (considered separately) one has the central mode $u_0 \neq 0$ with all other fields $u_n^k = v_n^k = 0$. On the other hand, when $\beta = 0$ [for $K = 3$ this case is illustrated in Fig. 1(c)], one readily obtains that there are $K + 1$ modes in the cluster composed of the central waveguide u_1 connected by α-bonds with K side waveguides v_1^k $(k = 1, \dots, K)$. $K - 1$ of these modes have $u_0 = 0$ and $v_1^1 + \cdots + v_1^K = 0$ where all v_1^k are constants, and correspond to zero eigenvalue. The two remaining modes are given by $u_0(z) = \pm u K^{1/2} e^{\pm i\alpha K^{1/2} z}$ and $v_1^1(z) = \cdots = v_1^K(z) = u e^{\pm i\alpha K^{1/2} z}$, where u is a constant.

In the general case $\alpha\beta > 0$ we address only the central localized modes, whose propagation constants b are outside the continuous spectrum given by $b^2(q) = \alpha^2 + \beta^2 + 2\alpha\beta\cos q$ (here it is assumed that all $u, v \propto e^{iqn + ib(q)z}$). Thus we look for a solution of (4) in the form

$$u_0 = u e^{ibz}, \quad u_n^k = u\sigma^n e^{-\lambda n + ibz}, \quad v_n^k = v^k \sigma^n e^{-\lambda n + ibz} \tag{5}$$

where $n \geq 1$, σ is either 1 or -1, constants v^k are to be found, and without loss of generality u is considered real. Notice that while u-waveguides in all rays have the same amplitudes, i.e., they do not depend on k, v-waveguides in different rays, generally speaking, have different amplitudes. Now the system (4) is reduced to

$$-bu = \alpha\sigma e^{-\lambda} \sum_{k=1}^{K} v^k \tag{6a}$$

$$-bv^k = \left(\beta + \sigma e^{\lambda}\alpha\right) u \tag{6b}$$

$$-bu = \left(\sigma e^{-\lambda}\alpha + \beta\right) v^k \tag{6c}$$

Taking into account that for the boundness of the modes one must impose $\lambda > 0$, one can distinguish two cases.

In the first case $\alpha < \beta$ [it generalizes the limit illustrated in Fig. 1(b)], one obtains one mode corresponding to $b = 0$, i.e., inside the gap of the continuous spectrum,

$$\sigma = -1, \quad v^{1,2,\dots,K} = 0, \quad u \neq 0, \quad \lambda = \ln\frac{\beta}{\alpha}. \tag{7}$$

This mode can be viewed as a generalization of the usual edge state of the SSH model in the topological phase to a star-junction.

In the second case, when $\alpha > \beta$ [it generalizes the limit illustrated in Fig. 1(c)], one can construct $K - 1$ linearly independent modes corresponding to $b = 0$:

$$\sigma = -1, \quad u = 0, \quad \sum_{k=1}^{K} v^k = 0, \quad \lambda = \ln\frac{\alpha}{\beta}. \tag{8}$$

Each such mode is determined by the respective set of amplitudes $(v^1, v^2, v^3, \dots, v^K)$. In particular one can choose them in the forms $(1, -1, 0, \dots, 0)$, $(1, 0, -1, \dots, 0)$, $\dots$, and $(1, 0, 0, \dots, -1)$. A remarkable fact is that the obtained solutions can also be interpreted as topological defect modes. While they do not have analogs in simple SSH chains, they exist in the SSH model with a multi-waveguide defect at one (or both) edges. Propagation constants of these modes also fall into the center of the gap and they disappear at $\alpha = \beta$, when the gap closes. The link between this case and the conventional finite SSH chain in a topological phase can be established by noting that for the described modes $u_0 = 0$, and effectively the rays are decoupled with the central site, while the most central waveguide of each of the rays is coupled

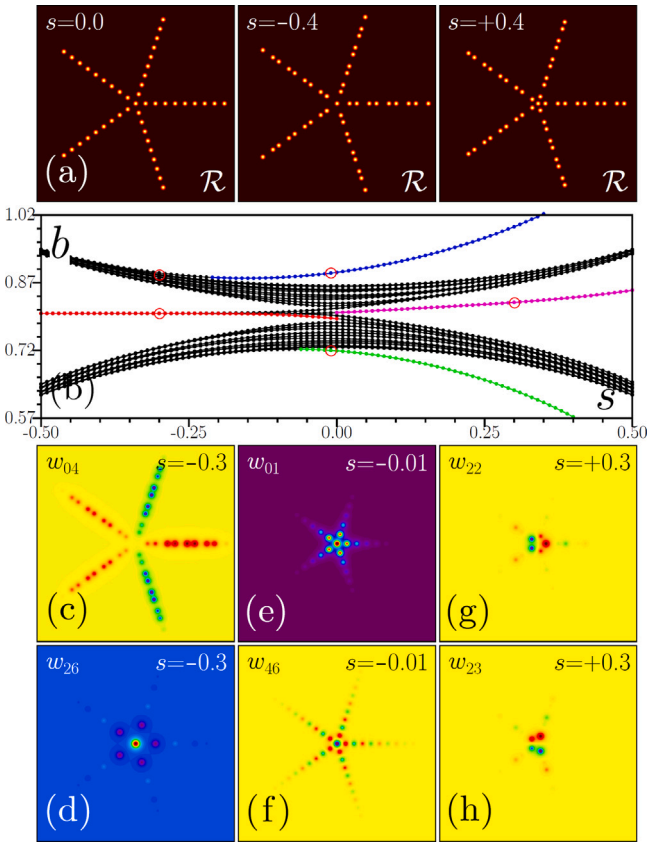

Fig. 4. Examples of arrays with $K = 5$ rays and $N = 5$ dimers (a), transformation of linear spectrum with shift s (b), and examples of eigenmodes (c)–(h).

to the rest of the ray by β. For $\alpha > \beta$ such edge of the chain supports a topological modes.

In this sense one can say, that the edge defect induces topology in the remainders of the rays (now viewed as started at v_1^k waveguides, i.e., excluding u_0-waveguide). To distinguish these two situations, the in-gap modes in the former case $\alpha < \beta$ will be termed as (usual) topological modes, while in the latter case $\alpha > \beta$, they will be referred to as defect-induced modes. All modes at the center of a gap should therefore have staggered tails.

Finally one can find defect modes in the semi-infinite gap, i.e., for $|b| > \alpha + \beta$. To this end we fix $\sigma = +1$ and look for a solution (6) with $v^1 = \cdots = v^K = v$ and $uv > 0$. Then from (6a) and (6c) we obtain the decay exponent for defect modes

$$\lambda = \ln \frac{\alpha(K-1)}{\beta} \tag{9}$$

while the propagation constants of such modes are given by

$$b = \pm(\alpha^2 + \beta^2 + 2\alpha\beta\cosh\lambda)^{1/2}. \tag{10}$$

These two modes exist for $\alpha(K-1) > \beta$. Interestingly, this means that for a star-junction with $K = 2$ these modes can co-exist only with defect-induced modes at $\alpha > \beta$, while for a star-junction with $K > 2$ they can coexist with usual topological modes in the parameter range $\alpha < \beta < \alpha(K-1)$. This provides a remarkable example of coexistence of topological and non-topological localized states in the center of the junction with $K = 3$ or more rays.

4. Modal spectrum of star-junctions

Turning now to numerical analysis of the fully 2D continuous model described by (1)–(3), we consider finite rays, representing SSH chains composed of N dimers (*alias* cells) where counting starts with the central waveguide. Topological properties of this system are controlled by the shift s. If $s < 0$ the coupling between waveguides inside each dimer (cell) becomes weaker than the coupling between waveguides from neighboring dimers, thus corresponding to the topologically phase (it corresponds to $\alpha < \beta$ in the above discrete model). At $s > 0$ we have the defect-induced topological phase (it corresponds to $\alpha > \beta$ in the above discrete model). Middle and right panels in Figs. 2(a)–4(a) below show examples of the respective star-junctions with $s \neq 0$.

To demonstrate qualitative modification of the linear spectrum of star-junctions upon variation of shift s, we omit the nonlinear term in Eq. (1) and address linear eigenmodes $\psi_n = w_n(\boldsymbol{r})e^{ib_n z}$, where $w_n(\boldsymbol{r})$ is a real function and b_n is the propagation constant. Due to large, but finite size of the junctions considered in numerics, all linear modes in such structures have size not exceeding the size of the star-junction and they all have positive propagation constants.

Strictly speaking, localized modes in a 2D Schrödinger equation, featuring discrete rotational symmetry, must be labeled by two mode indexes, one of which counts the eigenvalues, i.e., the propagation constants of the defect modes b_n of different types, while the second one would account for eventual degeneracy of an eigenvalues. However, because of the complexity of the problem, in particular due to different symmetries of the potential (2), (3) and that of the boundary conditions, numerically all obtained modes have distinct propagation constants (although the difference can be extremely small) and only one of the modes from the subspace determined by discrete rotations is shown. This allows us to sort the numerically obtained modes such that b_n decreases with increase of mode index n (i.e., to use a single scalar index to identify a mode).

Fig. 2(b) illustrates the transformation of the eigenvalue spectrum upon variation of shift s in the array with $K = 3$ rays. At $s < 0$ a gap opens in the spectrum that hosts four modes of topological origin: One of them indicated by the red dots is localized in the center of star-shaped array [Fig. 2(d)]. This central mode corresponds to the solution (7) for the discrete model, and it features all the properties of topological state predicted above: the light concentrates mainly in only one type of waveguides (belonging to one sublattice) and the mode is staggered, i.e., the sign of $w_n(\boldsymbol{r})$ changes on neighboring dimers in each array. The localization of topological mode increases with increase of $|s|$, while its propagation constant becomes practically independent of s even for moderate shifts, that is the natural consequence of the strong localization on scales smaller than the distance between neighboring waveguides. Three other modes, obtained for $s < 0$, form at the outer ends of each ray (due to the integer number of dimers) and we do not show them in the figure. In Fig. 2 bulk branches are shown by black dots in Fig. 2(b), the example of one such bulk mode is provided in Fig. 2(c).

Upon increase of the shift, the gap reopens and the spectrum at $s > 0$ hosts two types of defect-induced modes (that can be also considered as states of topological origin, as discussed above) with different internal structures depicted in Figs. 2(g) and 2(h) (other modes with similar internal structure can be obtained from the shown ones by rotation through the angle $2\pi/3$). These are 2D analogs of the central modes (8) obtained in the tight-binding approximation. The number of defect-induced modes in the gap at $s > 0$ depends on the number of rays in star-junction. While in the case of the tight-binding model there were $K - 1$ such modes [given by Eq. (8)], in the continuum model, this counting becomes more complicated.

The coexistence of the topological and non-topological defect modes branching out at some s from the upper and lower bulk bands was predicted by the tight-binding model [see (9) and (10)]. Now this is confirmed in full numerical simulations presented in Fig. 2(b) with blue and green dots. The peculiarity of the continuous model, however, is that the branch points for the upper and lower branches are generally speaking different [see also below]. In the case of three rays, they are close to the point $s = s_0 \approx -0.11$ [see Fig. 2(b)]. Unlike topological

modes, non-topological defect states have light in each waveguide. In modes from the upper (blue) branch the field is in-phase in all waveguides [Fig. 2(e)], while in modes from the lower (green) branch the field changes its sign between neighboring waveguides [Fig. 2(f)]. Localization of these modes gradually increases with increase of $s > s_0$ [cf. Eq. (9)]. Notice that non-topological branches, depicted by blue and green lines in Fig. 2(b), remain for $s > 0$. The physical reason for localization of the modes of the types shown in Fig. 2(e)–(h) can be viewed as geometry-mediated local increase of the density of waveguides in the center of star-junction.

Similar transformation of linear spectrum with s is encountered in structures with $K = 4$ (Fig. 3) and $K = 5$ (Fig. 4) rays. All of them host single topological mode in the center of the star-junction at $s < 0$ that co-exists with topological modes at outer ends of the rays. The richness of shapes of topological modes increases with increase of the number of rays K in the structure [cf. Figs. 3(d) and 4(d)]. As peculiarities of the continuum model, as compared with its tight-binding approximation, we notice that with increase of the number of rays in our continuous model the coupling between non-central waveguides belonging to different rays comes into the play, leading to gradual upward shift of the $b_n(s)$ curves. Moreover, increase of K leads to notable difference in bifurcation points (values of s) at which defect mode branches shown with blue and green dots in Figs. 3(b) and 4(b) emerge from bulk bands. This difference is particularly well visible for $K = 5$ array. In the $K = 5$ array there are two types of defect-induced modes in the finite gap. Their examples are shown in Fig. 4(g) and Fig. 4(h).

Unlike in the discrete model, in the defect-induced topological phase, now the value and degeneracy of the propagation constants depend on both s and K that occurs due to increasing strength of evanescent coupling between waveguides belonging to neighboring arrays (this effect is not accounted for by the discrete model). One can see that propagation constants of defect-induced in-gap modes slightly change with s, this is particularly visible for $K = 5$ junction [Fig. 4(b), cf. the magenta branches in this figure and in Fig. 2(b) for $K = 3$]. An unexpected result is shown in Fig. 3(b) where in the case of even number of waveguides, $K = 4$, there appear two branches of the defect-induced modes, see magenta and dark yellow dots. Furthermore, one of these branches, the dark yellow one, is notably shifted into lower part of the finite gap when s increases. For $K = 4$ the branch shown by magenta dots represents eigenvalues of dipole-like modes [an example is shown in Fig. 3(g)]. The lower branch of the defect-induced modes (dark yellow dots) correspond to quadrupole-type modes.

5. Solitons in star-junctions

Now we turn to the properties of nonlinear modes (*alias* solitons) that bifurcate from the linear defect modes. We thus take into account nonlinear term in Eq. (1) and look for soliton solutions in the form $\psi(\boldsymbol{r}, z) = w(\boldsymbol{r})e^{ibz}$. Now the propagation constant b parameterizes a soliton family and determines the dependence $U(b)$, where $U = \iint |w|^2 d^2\boldsymbol{r}$ is the total soliton power. We first consider solitons emerging in the usual topological phase, at $s < 0$, and residing in the center of the star-junction. As usual, in a focusing media, amplitudes and powers of such states increase away from the bifurcation point, where propagation constant coincides with the eigenvalue of the linear mode [the dashed vertical line in Fig. 5(a)] that are practically identical in the star-junctions with different number of rays K. In the focusing nonlinear medium considered here, upon increase of the nonlinearity, the soliton propagation constant shifts towards the top of the allowed band [right gray region in Fig. 5(a)], and enters the allowed gap where it coexists with delocalized bulk modes that is accompanied by a rapid growth of the total power. This increase of the power inside the gap occurs due to increasing extension of the solitons across array [cf. solitons near the bifurcation point in Figs. 5(b), (d), and (f) with the respective shapes close to the allowed band in Figs. 5(c), (e), and (g)].

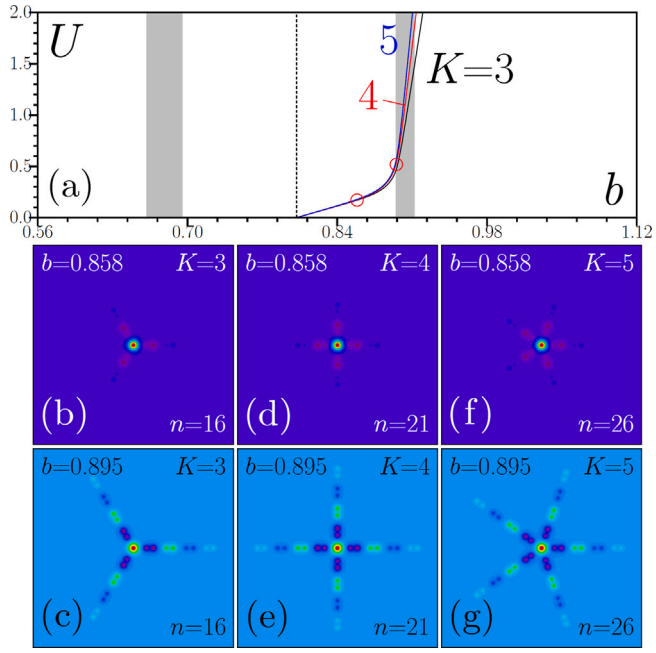

Fig. 5. (a) Power of topological solitons bifurcating from linear topological state, whose eigenvalue is marked by the dashed line, versus propagation constant b in star-junctions with $s = -0.4$ and different number of rays K. Gray regions correspond to bulk bands of linear spectrum. (b)–(g) Soliton profiles corresponding to the red circles in (a) in structures with different number of rays K. Indices of linear modes from which bifurcation occurs are indicated on the profiles.

Solitons, in general, inherit the internal structure of linear topological modes, but in nonlinear regime both waveguides in the central dimers become populated. Discrete rotational symmetry of topological solitons is determined by discrete rotational symmetry of corresponding array. Remarkably, analysis of stability that was performed using direct propagation in the frames of Eq. (1) of weakly perturbed by broad-band input noise solitons has shown that for our parameters whole families of topological solitons for any number of rays K in the array are stable, even when such states couple with modes in the band, becoming delocalized.

In the defect-induced topological phase, at $s > 0$, soliton families are richer, because in this phase linear spectrum contains several localized modes with different internal structure and in different gaps, from which soliton families can bifurcate. Representative $U(b)$ dependencies for solitons in $K = 3$ array are presented in Fig. 6. In the top semi-infinite gap increasing with b nonlinearity leads to progressive localization of the non-topological soliton and its eventual contraction to the central waveguide [see example in Fig. 6(b)]. In contrast, non-topological soliton from the bottom gap that bifurcates from defect mode with staggered tails becomes more extended when b increases [Fig. 6(g)], and delocalizes when b enters lower band (left gray region). The non-topological defect solitons in the top and bottom gaps are completely stable. In finite gap one finds two types of defect-induced solitons with different internal structures [Figs. 6(c) and 6(e)]. Each such family has degeneracy K with other nonlinear modes obtained by the rotation through the angle $2\pi/K$. When such solitons shift into the top band [right gray region in Fig. 6(a)], one of them extends along all three rays [Fig. 6(d)], while the other soliton extends along two rays only, with no light in the third ray [Fig. 6(f)]. These two families feature very different stability properties. Solitons bifurcating from linear mode with index $n = 14$ depicted in Figs. 6(c) and 6(d) are stable only near bifurcation point and become unstable even at moderate powers [in Fig. 6 stable (unstable) families are shown with black (red) color]. In contrast, solitons bifurcating from mode with $n = 15$ [Figs. 6(e) and 6(f)] are always stable.

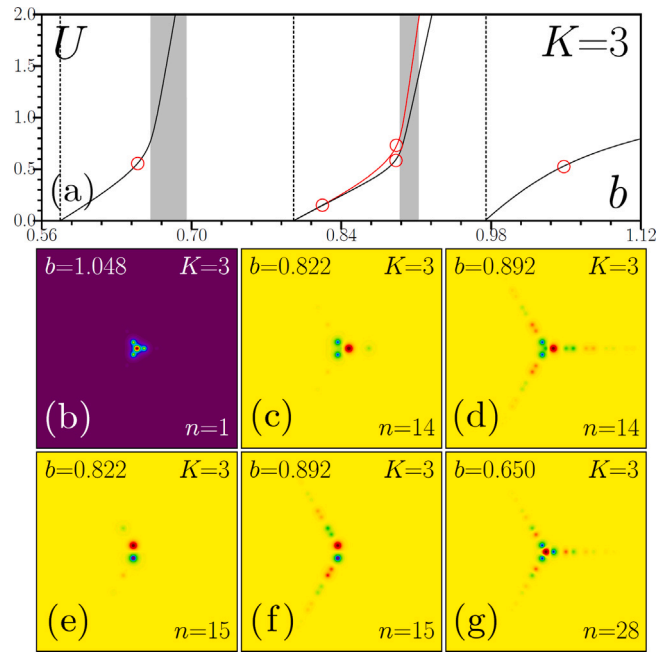

Fig. 6. (a) Families of solitons bifurcating from different defect modes if star-junction with $K = 3$ rays with $s = +0.4$. (b)–(g) Examples of solitons corresponding to the red circles in (a). Black families correspond to stable solitons; red families correspond to unstable solitons.

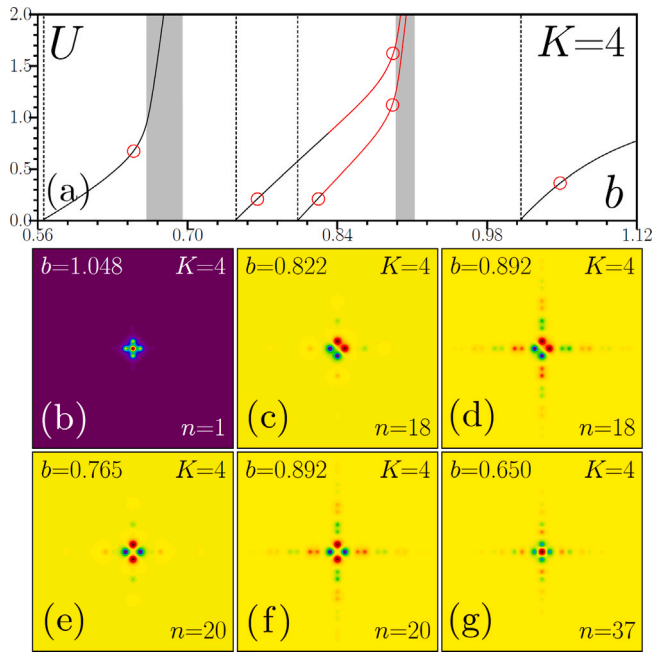

Fig. 7. (a) Families of solitons bifurcating from different linear modes in a star-junction with $s = +0.4$ and $K = 4$. (b)–(g) Examples of solitons corresponding to the red circles in (a). Black branches correspond to stable solitons; red branches correspond to unstable solitons.

Families of solitons in a star-junction with $K = 4$ rays are presented in Fig. 7(a). As in the previous case, two families of stable defect non-topological solitons, shown in Figs. 7(b) and (g), bifurcate towards the top semi-infinite and bottom gaps. Two families of defect-induced solitons, formed in the finite gap have different symmetry and bifurcate from linear modes with different propagation constants. Among them, quadrupole-like solitons are stable in considerable part of the gap at lower amplitudes, but become unstable at higher amplitudes [Figs. 7(e) and 7(f)]. The family of the dipole-like solitons from Figs. 7(c) and 7(d) is stable only near the bifurcation point, and becomes unstable even at moderate amplitudes.

We also considered star-junctions with $K = 5$ and larger number of rays. In all the cases we observe a general situation when a linear defect mode gives origin to a nonlinear family. The general tendency with existence of single stable soliton family at $s < 0$, and several families with distinct stability properties (especially in finite gap) at $s > 0$ is observed in such structures as well. To confirm the stability results, in Fig. 8 we show a typical example of the stable propagation of a perturbed topological soliton at $s = -0.4$ [Fig. 8(a)]. The unstable in-gap state in defect-induced topological phase at $s = +0.4$ demonstrates gradually increasing oscillations of central spots that are accompanied by radiation and eventual expansion of soliton [Fig. 8(b)]. Stable defect-induced soliton at the same propagation constant maintains its shape over very long distances, even when it is perturbed [Fig. 8(c)].

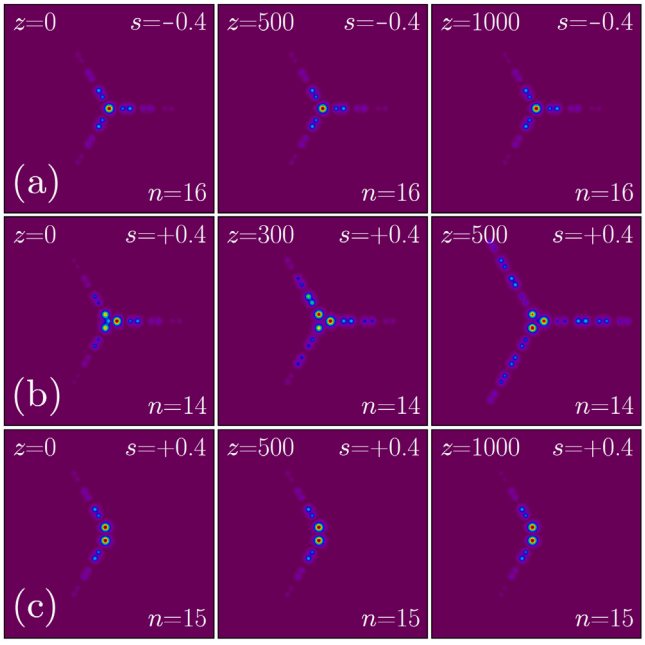

Fig. 8. Stable propagation of a perturbed topological soliton at $s = -0.4$ (a), decay of an unstable defect-topological soliton at $s = +0.4$ (b), and stable propagation of a defect-topological soliton at $s = +0.4$ (c) in star-shaped SSH arrays with $K = 3$ rays. All solitons correspond to $b = 0.89$, the index of linear modes from which they bifurcate is indicated on each panel.

6. Modes in junctions with structural defects

To confirm that the in-gap modes in a star-junction have topological origin and that they are not affected by deformations of the structure, we introduced perturbation into the $K = 3$ array that breaks its three-fold discrete rotational symmetry — namely, we removed three outermost waveguides from one of the rays of the structure, as shown in Figs. 9(b) and 9(c). Comparing the linear spectra of deformed [Fig. 9(a)] and original [Fig. 9(e)] arrays, we observe that the very existence of the in-gap modes in the center of star-junction is not affected. The difference between topological ($s < 0$) and defect-induced ($s > 0$) modes consists in emergence of additional branches inside the gap, which appear due to the introduced defect. As expected, when a defect mode is strongly localized, it remains very weakly affected by the introduced defect [c.f. Figs. 9(d) and 2(d); the mode numbers are different because of different numbers of modes in these cases]. Clearly, for small $|s| \to 0$, when widths of the modes are comparable with the size of the structure, the deformation manifests in asymmetry of the

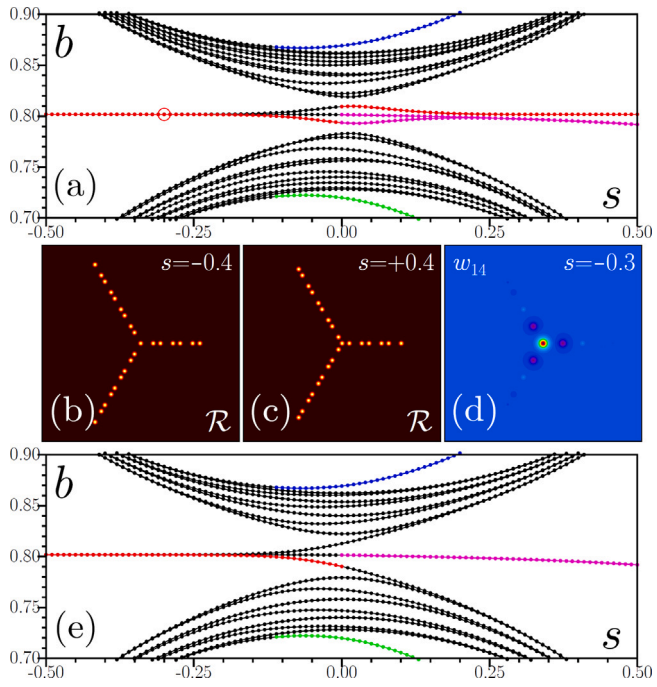

Fig. 9. Comparison of the linear spectrum of (a) star-shaped arrays with 3 removed waveguides in the horizontal ray, as shown in (b) and (c) for $s = -0.4$ and $s = 0.4$, respectively, with the spectrum of (e) the star-junction with rays of equal length. (d) Example of a topological mode at $s = -0.3$ corresponding to the red dot in (a). Here $K = 3$.

mode. Because we removed odd number of waveguides, the modified ray acquires a "topological edge" at $s > 0$ [Fig. 9(c)], thus hosting a standard SSH topological mode at its outer end: this mode is clearly visible in spectrum at $s > 0$ [red dots at $s > 0$ in Fig. 9(a)].

7. Conclusions

Summarizing, we have shown that SSH chains arranged in two-dimensional star-shaped configuration with properly chosen parameters of the waveguides, allow for existence of three types of the central modes. The first one is an extension of the conventional topological edge states in the SSH arrays, which survives in the presence of several rays. The propagation constant of such mode is located in spectral gap. The second type of the modes (there are several of them) with the propagation constants in the gap can be viewed as the defect-introduced topological modes. They also have analogs in the conventional SSH chains with a defect site on the one side of the chain. The two types of the modes occur at different parameters of the rays, and disappear when coupling constants between all waveguides become equal. Finally, there are defect modes localized in the center of the star-junction whose propagation constants are located above and below the top and bottom bands of the continuous spectrum. Each type of the linear defect mode gives origin to a family of nonlinear modes enabled by the focusing nonlinearity, which can be stable for large range of the junction parameters and amplitude of the modes.

CRediT authorship contribution statement

Yaroslav V. Kartashov: Conceptualization, Investigation, Software, Writing – original draft, Writing – review & editing. **Vladimir V. Konotop:** Conceptualization, Formal analysis, Investigation, Writing – original draft, Writing – review & editing.

Declaration of competing interest

Authors declare that they have no conflict of interest.

Data availability

Data used for preparation of figures in this paper are available from the corresponding author upon reasonable request.

Acknowledgments

The authors are very grateful to Dr. S. K. Ivanov for fruitful discussion of these results and numerical support.

The work of Y.V.K. was supported by the research project FFUU-2021-0003 of the Institute of Spectroscopy of the Russian Academy of Sciences, Russia.

The work of V.V.K. was supported by the Portuguese Foundation for Science and Technology (FCT), Portugal under Contracts PTDC/FIS-OUT/3882/2020 (DOI: 10.54499/PTDC/FIS-OUT/3882/2020) and UIDB/00618/2020 (DOI: 10.54499/PTDC/FIS-OUT/3882/2020).

References

[1] McGurn AR. Photonic crystal circuits: Localized modes and waveguide couplers. Phys Rev B 2002;65:075406.
[2] McGurn AR, Birkok G. Transmission anomalies in Kerr media photonic crystal circuits: Intrinsic localized modes. Phys Rev B 2004;69:235105.
[3] Burioni R, Cassi D, Sodano P, Trombettoni A, Vezzani A. Opological filters and high-pass/low-pass devices for solitons in inhomogeneous networks. Phys Rev E 2006;73:066624.
[4] Heinrich M, Keil R, Dreisow F, Tünnermann A, Nolte S, Szameit A. Nonlinear localized states in the vicinity of topological defects in waveguide arrays. New J Phys 2010;12:113020.
[5] Keil R, Heinrich M, Dreisow F, Pertsch T, Tünnermann A, Nolte S, et al. All-optical routing and switching for three-dimensional photonic circuitry. Sci Rep 2011;94:1.
[6] Kevrekidis PG, Frantzeskakis DJ, Theocharis G, Kevrekidis IG. Guidance of matter waves through Y-junctions. Phys Lett A 2003;317:513–22.
[7] Miroshnichenko AE, Molina MI, Kivshar YS. Localized modes and bistable scattering in nonlinear network junctions. Phys Rev E 2007;75:046602.
[8] Stojanović M, Maluckov A, Hadžievski Lj, Malomed BA. Surface solitons in trilete lattices. Physica D 2011;240:1489.
[9] Kottos T, Smilansky U. Quantum chaos on graphs. Phys Rev Lett 1997;79:4794–7.
[10] Shafei S, Lytel R, Kuzyk MG. Geometry-controlled nonlinear optical response of quantum graphs. J Opt Soc Amer B 2012;29:3419.
[11] Lytel R, Shafei S, Smith JH, Kuzyk MG. Influence of geometry and topology of quantum graphs on their nonlinear optical properties. Phys Rev A 2013;87:043824.
[12] Gnutzmann S, Waltner D. Stationary waves on nonlinear quantum graphs: General framework and canonical perturbation theory. Phys Rev E 2016;93:032204.
[13] Noja D. Nonlinear Schrödinger equation on graphs: recent results and open problems. Phil Trans R Soc A 2023;372:20130002.
[14] Kartashov YV, Konotop VV, Vysloukh VA, Zezyulin DA. Guided modes and symmetry breaking supported by localized gain. In: Malomed B, editor. Spontaneous symmetry breaking, self-trapping, and josephson oscillations. Progress in optical science and photonics, Vol. 1, Berlin, Heidelberg: Springer; 2012.
[15] Xu HS, Xie LC, Jin L. High-order spectral singularity. Phys Rev A 2023;107:062209.
[16] Su WP, Schrieffer JR, Heeger AJ. Solitons in polyacetylene. Phys Rev Lett 1979;42:1698–701.
[17] Ozawa T, Price HM, Amo A, Goldman N, Hafezi M, Lu L, et al. Topological photonics. Rev Modern Phys 2019;91:015006.
[18] Smirnova D, Leykam D, Chong Y, Kivshar Y. Nonlinear topological photonics. Appl Phys Rev 2020;7:021306.
[19] Kim M, Jacob Z, Rho J. Recent advances in 2D, 3D and higher-order topological photonics. Light Sci Appl 2020;9:130.
[20] Schomerus H. Topologically protected midgap states in complex photonic lattices. Opt Lett 2013;38:1912.
[21] Arkhipova AA, Ivanov SK, Zhuravitskii SA, Skryabin NN, Dyakonov IV, Kalinkin AA, et al. Observation of nonlinearity-controlled switching of topological edge states. Nanophot 2022;11:3653.
[22] Ivanov SK, Zhuravitskii SA, Skryabin NN, Dyakonov IV, Kalinkin AA, Kulik SP, et al. Macroscopic zeno effect in a su-schrieffer-heeger photonic topological insulator. Laser Phot Rev 2023;17:202300024.
[23] Sivan A, Orenstein M. Topology of multiple cross-linked Su-Schrieffer-Heeger chains. Phys Rev A 2022;106:022216.
[24] Lumer Y, Plotnik Y, Rechtsman MC, Segev M. Self-localized states in photonic topological insulators. Phys Rev Lett 2013;111:243905.
[25] Ablowitz MJ, Curtis CW, Ma Y-P. Linear and nonlinear traveling edge waves in optical honeycomb lattices. Phys Rev A 2014;90:023813.

[26] Leykam D, Chong YD. Edge solitons in nonlinearphotonic topological insulators. Phys Rev Lett 2016;117:143901.
[27] Kartashov YV, Skryabin DV. Modulational instability and solitary waves in polariton topological insulators. Optica 2016;3:1228.
[28] Ablowitz MJ, Cole JT. Tight-binding methods for general longitudinally driven photonic lattices: Edge states and solitons. Phys Rev A 2017;96:043868.
[29] Ivanov SK, Kartashov YV, Szameit A, Torner L, Konotop VV. Vector topological edge solitons in Floquet insulators. ACS Photon 2020;7:735.
[30] Zhang ZY, Wang R, Zhang YQ, Kartashov YV, Li F, Zhong H, et al. Observation of edge solitons in photonic graphene. Nature Commun 2020;11:1902.
[31] Ivanov SK, Kartashov YV, Heinrich M, Szameit A, Torner L, Konotop VV. Topological dipole Floquet solitons. Phys Rev A 2021;103:053507.
[32] Zhong H, Xia S, Zhang Y, Li Y, Song D, Liu C, et al. Nonlinear topological valley Hall edge states arising from type-II Dirac cones. Adv Photon 2021;3:056001.
[33] Ren B, Wang H, Kompanets VO, Kartashov YV, Li Y, Zhang Y. Dark topological valley hall edge solitons. Nanophoton 2021;10:3559.
[34] Hang C, Zezyulin DA, Huang G, Konotop VV. Nonlinear topological edge states in a non-Hermitian array of optical waveguides embedded in an atomic gas. Phys Rev A 2021;103:L040202.
[35] Mukherjee S, Rechtsman MC. Observation of Floquet solitons in a topological bandgap. Science 2020;368:856.
[36] Maczewsky LJ, Heinrich M, Kremer M, Ivanov SK, Ehrhardt M, Martinez F, et al. Nonlinearity-induced photonic topological insulator. Science 2020;370:701.
[37] Mukherjee S, Rechtsman MC. Observation of unidirectional solitonlike edge states in nonlinear Floquet topological insulators. Phys Rev X 2021;11:041057.
[38] Kirsch MS, Zhang Y, Kremer M, Maczewsky LJ, Ivanov SK, Kartashov YV, et al. Nonlinear second-order photonic topological insulators. Nat Phys 2021;17:995.
[39] Hu Z, Bongiovanni D, Jukic D, Jajtic E, Xia S, Song D, et al. Nonlinear control of photonic higher-order topological bound states in the continuum. Light Sci Appl 2021;10:164.
[40] Ren B, Arkhipova AA, Zhang Y, Kartashov YV, Wang H, Zhuravitskii SA, et al. Observation of nonlinear disclination states. Light: Sci Appl 2023;12:194.
[41] Gorlach MA, Slobozhanyuk AP. Nonlinear topological states in the Su–Schrieffer–Heeger model. Nanosyst: Phys Chem Math 2017;8:695.
[42] Solnyshkov DD, Bleu O, Teklu B, Malpuech G. Chirality of topological gap solitons in bosonic dimer chains. Phys Rev Lett 2017;118:023901.
[43] Dobrykh DA, Yulin AV, Slobozhanyuk AP, Poddubny AN, Kivshar YuS. Nonlinear control of electromagnetic topological edge states. Phys Rev Lett 2018;121:163901.
[44] Chaunsali R, Xu HT, Yang JY, Kevrekidis PG, Theocharis G. Stability of topological edge states under strong non-linear effects. Phys Rev B 2021;103:024106.
[45] Xia SQ, Jukic D, Wang N, Smirnova D, Smirnov L, Tang LQ, et al. Nontrivial coupling of light into a defect: the interplay of nonlinearity and topology. Light: Sci Appl 2020;9:147.
[46] Guo M, Xia SQ, Wang N, Song DH, Chen ZG, Yang JK. Weakly nonlinear topological gap solitons in Su-Schrieffer-Heeger photonic lattices. Opt Lett 2020;45:6466.
[47] Kartashov YV, Arkhipova AA, Zhuravitskii SA, Skryabin NN, Dyakonov IV, Kalinkin AA, et al. Observation of edge solitons in topological trimer arrays. Phys Rev Lett 2022;128:093901.
[48] Zhong H, Kartashov YV, Li Y, Zhang Y. π-Mode solitons in photonic Floquet lattices. Phys Rev A 2023;107:L021502.
[49] Arkhipova AA, Zhang Y, Kartashov YV, Zhuravitskii SA, Skryabin NN, Dyakonov IV, et al. Observation of π-solitons in oscillating waveguide arrays. Sci Bull 2023;68:2017.
[50] Landau LD, Lifshitz EM. Quantum mechanics (non-relativistic theory). Butterworth-Heinemann; 1981.
[51] Simon B. The bound state of weakly coupled Schrödinger operators in one and two dimensions. Ann Physics 1976;97:279.
[52] Szameit A, Nolte S. Discrete optics in femtosecond-laser-written photonic structures. J Phys B: At Mol Opt Phys 2010;43:163001.
[53] Asbóth JK, Oroszlany L, Palyi A. A short course on topological insulators. Springer International Publishing Switzerland; 2016.